Desalination and Water Treatment
www.deswater.com

doi: 10.5004/dwt.2017.21110

81 (2017) 143–151
June

Preparation of chitosan-*graft*-benzo-15-crown-5 ether film for heavy metal ions separation

Mingxia Wang[a,b], Feng Yan[a,c,*], Zhou Fang[c,d], Yuzhong Zhang[a,b]

[a]*State Key Laboratory of Separation Membranes and Membrane Processes/National Center for International Joint Research on Separation Membranes, Tianjin Polytechnic University, Tianjin 300387, P. R. China, Tel. +86 2283955451; email: yanfeng.yxm@hotmail.com (F. Yan), Tel. +86 2283955074; emails: esmbee@163.com (M. Wang), zhangyz2004cn@vip.163.com (Y. Zhang)*
[b]*School of Materials Science and Engineering, Tianjin Polytechnic University, Tianjin 300387, P. R. China*
[c]*School of Environmental and Chemical Engineering, Tianjin Polytechnic University, Tianjin 300387, P. R. China*
[d]*Tianjin Special Equipment Inspection Institute, Tianjin 300192, China, Tel. +86 2223366633; email: 826193810@qq.com*

Received 13 January 2017; Accepted 2 July 2017

ABSTRACT

Chitosan-*graft*-benzo-15-crown-5 ether (CTS-*g*-B15C5) for metal ion separation was prepared and optimized by Box–Behnken design (BBD). Results showed that the maximum immobilization amount (I_A) of crown ether grafting on chitosan (CTS) polymer was 4.93 mmol·g^{-1} under the optimal conditions, which is in good agreement with the result predicted by BBD (4.97 mmol·g^{-1}). Moreover, the CTS-*g*-B15C5 film exhibited an excellent adsorption ability and selectivity to different metal ions. The adsorption rates obtained by CTS-*g*-B15C5 film were 96.9% for Ag^+ and 94.3% for Pd^{2+}, which were higher than those obtained by CTS at the similar conditions. The order of adsorption ability on CTS-*g*-B15C5 was $Ag^+ > Pd^{2+} > Pb^{2+} > Cu^{2+} > Ni^{2+} > Cr^{3+}$, and the selectivity coefficients of CTS-*g*-B15C5 for metal ions were $K_{Ag^+/Ni^{2+}}$ = 5.40, $K_{Ag^+/Cr^{3+}}$ = 8.59, and $K_{Pd^{2+}/Cr^{3+}}$ = 8.44, respectively. The results showed that CTS-*g*-B15C5 film could be used for separation of precious metals Ag^+ and Pd^{2+}. Furthermore, the CTS-*g*-B15C5 film could be reused after regeneration, and the adsorption rates for Ag^+ and Pd^{2+} kept up to 90% after being regenerated for five times, which suggests a good stability and potential application in heavy metal recycling field.

Keywords: Chitosan; Benzo-15-crown-5 ether; Heavy metal ion; Separation

1. Introduction

Contamination of toxic heavy metals is now a serious environmental problem that significantly affects the quality of water supply [1]. Effluents from industry, such as printing and dyeing, metallurgy, electroplating, and mining are the main sources containing heavy metals. Toxic heavy metals, such as lead, nickel, mercury, cadmium, and copper, cause severe damages to human health [2–4]. Hence, it is important to remove metal ions from industrial wastewater as well as drinking water. Convention treatment processes such as chemical precipitation [5], oxidation/reduction [6], adsorption [7], ion-exchange [8], membrane separation [9], and electrochemical removal [10] are widely used for removing the toxic heavy metals. Among them, adsorption especially using low-cost adsorbents is one of the economical and effective methods for metal contamination removal [11]. Bailey et al. [12] summarized an extensive list of low-cost sorbents including chitosan (CTS), xanthate, zeolite, etc., for removal of heavy metals. Among the 12 identified potential sorbents, CTS exhibits the highest sorption capacity for copper, lead, mercury, and zinc.

CTS, a poly-*N*-acetylglucosamine, is normally obtained from alkaline deacetylation of chitin, and is the second natural organic polymer next to cellulose in abundance [13]. It is extensively used for heavy metal removal from aqueous solution due to the composition of amine and abundant

* Corresponding author.

hydroxyl groups [14–17]. However, $-NH_2$ is easily protonated in acid, which results in CTS dissolving and losing in water. Furthermore, CTS adsorption is non-selective separation of metal ions and requires chemical modification to improve its selectivity for target ions [18,19]. A number of strategies have been proposed to enhance the adsorption capacity and selectivity of CTS for heavy metal ions, such as modifying CTS with magnetic particles [20,21], synthesizing ethylenediamine-type CTS with more N-coordination sites [22], preparing CTS-based hydrogels [23,24], and grafting with crown ether [25]. Among them, crown ether graft CTS seems to be a promising way to enhance the selectivity of CTS.

Crown ethers are an integral part of many receptors that can be called "molecular mousetraps" as they have the ability to bind the positively charged guest. They show selectively complexing with metal ions due to the particular molecular structures. For example, benzo-15-crown-5 ether (B15C5) is known to binding Na^+, K^+, and Ag^+ ions reversibly [26]. However, free crown ethers are toxic, and not easily to be recovered after being used. Strategies of grafting crown ether onto CTS polymer have been presented to solve the problem. Ding et al. [25] reported a *N,N*′-dibenzo-18-crown-6 ether graft chitosan (CTSDC), which was further cross-linked by epichlorohydrin to present diazacrown ether cross-linked chitosan (CCTSDC). Both CTSDC and CCTSDC show good performance for adsorbing noble metal ions and high selectivity for adsorption of Ag^+ and Pd^{2+}.

In our previous work, B15C5 was grafted onto CTS polymer [27]. It was found that the immobilized crown ether showed good performance for lithium isotope separation and the separation factor was 1.037. However, the reaction condition of the graft process has not been explored and the adsorption for heavy metal ions has not been studied in detail. The aim of the present study is to optimize the reaction parameters for preparing the chitosan-*graft*-benzo-15-crown-5 ether (CTS-*g*-B15C5), and explore the performances of CTS-*g*-B15C5 for heavy metal ions separation.

2. Materials and methods

2.1. Materials

CTS was obtained from National Pharmaceutical Group Corporation (China). The degree of deacetylation is 83.2% (determined by ^{1}H NMR [28]). 4′-Formylbenzo-15-crown-5 ether (FB15C5) was synthesized by the method reported in the literature [29] and its structure was confirmed by Fourier transform infrared spectroscopy and ^{1}H NMR spectra. All other reagents were purchased from Tianjin Guangfu Fine Chemical Research Institute (China).

2.2. Preparation of chitosan-graft-benzo-15-crown-5 ether

CTS-*g*-B15C5 polymer was synthesized through the Schiff base reaction between the amino groups of CTS and the formyl groups of FB15C5 as the previous work [24]. Typically, FB15C5 was dissolved in a certain volume of ethanol (*V*, mL), and a definite amount of CTS (0.5 g) was dissolved in a certain concentration of acetic acid aqueous solution ($V' = V$). The FB15C5 solution was added dropwise into the mixture over 30 min in a nitrogen atmosphere, and was refluxed under stirring for 24 h. Then, the pH of the solution was adjusted to 7.0 by sodium hydroxide solution (1.0 mol·L^{-1}) to end the reaction. The mixture was distilled under vacuum and washed with distilled water. Finally, the Schiff base type CTS-*g*-B15C5 polymer was obtained after being extracted with ethanol (300 mL) in a Soxhlet apparatus. The degree of substitution (DS) is determined by Eq. (1) and the immobilized amount (I_A; mmol·g^{-1}) of crown ether is determined by Eq. (2):

$$\frac{m \times w}{14} = \frac{m}{(M_{CTS} \times (1 - DS) + M_{CTS-g-B15C5} \times DS) \times 83.2\% + M_{CT} \times 16.8\%} \quad (1)$$

$$I_A = \frac{DS}{M_{CTS}} \times 1000 \quad (2)$$

where m (g) denotes the mass of CTS-*g*-B15C5 polymer; w (wt%) is the weight fraction of N of CTS-*g*-B15C5 (obtained by elemental analysis, Vario EL Cube Automatic Instrument, Germany); $M_{CTS,}$ $M_{CTS-g-B15C5}$, and M_{CT} are the molar mass of CTS units, CTS-*g*-B15C5 units, and undeacetylated chitin units on the polymer molecules, respectively. The chemical structure of CTS-*g*-B15C5 was characterized by solid-state ^{13}C nuclear magnetic resonance (^{13}C NMR, Varian Infinity plus 300WB NMR spectrometer).

2.3. Response surface methodology design for preparing CTS-g-B15C5

Response surface methodology (RSM) was employed to optimize the experimental parameters, and Box–Behnken design (BBD) was selected as experimental design techniques due to its advantages for a quadratic response surface model with three or more factors [30,31]. According to the results obtained from single factor experiments [24], four reaction parameters including crown ether amount (*A*, g), ethanol amount (*B*, mL), acetic acid concentration (*C*, v/v %), and reaction time (*D*, h), were selected as variables for the experimental design of BBD (three-level-four-factor). The experimental design including independent factors (*A*–*D*) and levels were shown in Table 1. A total of 29 RSM arrangements with different variables were prepared according to experimental design for four-factor system with five replicates at the center point (Table 2). Analysis of variance (ANOVA) was used to evaluate the fitness of the model.

Table 1
Independent variables and their levels used for RSM

Variables	Levels		
	–1	0	+1
Crown ether amount (*A*), g	1.1	1.3	1.5
Ethanol amount (*B*), mL	20	30	40
Acetic acid concentration (*C*), v/v %	8	12	16
Reaction time (*D*), h	21	24	27

Table 2
RSM arrangement and responses for the immobilized amount of crown ether[a]

Run	Variables				Observed value I_A (mmol·g^{-1})
	A (g)	*B* (mL)	*C* (v/v %)	*D* (h)	
1	1.3	30	12	24	4.86
2	1.3	30	8	21	4.94
3	1.3	40	12	21	4.50
4	1.3	30	12	24	4.71
5	1.5	30	16	24	4.31
6	1.3	30	12	24	4.86
7	1.1	40	12	24	3.95
8	1.3	20	8	24	4.50
9	1.3	20	12	27	4.56
10	1.3	30	16	27	4.38
11	1.5	30	8	24	4.85
12	1.5	20	12	24	4.38
13	1.3	30	12	24	4.71
14	1.1	30	16	24	4.62
15	1.1	30	12	21	4.59
16	1.1	20	12	24	4.40
17	1.5	30	12	21	4.38
18	1.3	30	16	21	4.59
19	1.3	40	8	24	4.87
20	1.3	20	16	24	4.74
21	1.5	30	12	27	4.79
22	1.1	30	12	27	4.10
23	1.3	40	12	27	4.01
24	1.3	20	12	21	4.80
25	1.3	40	16	24	4.47
26	1.5	40	12	24	4.36
27	1.3	30	12	24	4.46
28	1.3	30	8	27	4.70
29	1.1	30	8	24	4.63

[a]*A*, crown ether amount; *B*, ethanol amount; *C*, acetic acid concentration; *D*, reaction time; I_A, immobilized amount of crown ether on CTS.

2.4. The adsorption experiments

2.4.1. The adsorption performance of FB15C5

The adsorption performance of FB15C5 was studied by liquid–liquid extraction. An aqueous solution containing heavy metal ions such as Pb^{2+}, Ag^{+}, Pd^{2+}, Ni^{2+}, Cu^{2+}, and Cr^{3+} was prepared from analytical grade metal nitrates. The concentration of each metal ion was 0.01 mol·L^{-1}. 10 mL FB15C5 chloroform solution (0.01 mol·L^{-1}) and 10 mL aqueous solution of heavy metal ions were mixed together at a bottomed flask and stirred for 90 min. Then, the concentration of metal ions in aqueous phase after extraction was measured with an inductively coupled plasma optical emission spectroscopy (ICP-OES; Varian, 715-ES, American).

2.4.2. The adsorption performance of CTS and CTS-*g*-B15C5 films

The CTS and CTS-*g*-B15C5 films were prepared as follows: 2 g CTS or CTS-*g*-B15C5 polymer was dissolved in 18 mL (v/v %) acetic acid aqueous solution. After deaerating, the homogenous mixture was poured onto a clean glass plate, and air-dried overnight. The obtained film was washed by 5 wt% sodium carbonate solution and water, and dried under vacuum.

The adsorption performances of CTS and CTS-*g*-B15C5 films were conducted by a liquid–solid extraction. 0.1 g CTS or CTS-*g*-B15C5 film was added into a flask with 25 mL heavy metal ions aqueous solution, which contains Pb^{2+}, Ag^{+}, Pd^{2+}, Ni^{2+}, Cu^{2+}, and Cr^{3+} ions. The concentration of each metal ion was 25 mg·L^{-1} at pH 4 [25,32]. The liquid–solid mixture was stirred for 12 h. After filtration, the ion concentration in the solution was determined by ICP-OES. The adsorption amount (Q) and adsorption rate (q) for each ion at equilibrium were calculated by Eqs. (3) and (4), respectively:

$$Q = \frac{(C_o - C_e) \times V}{m} \tag{3}$$

$$q = \frac{(C_o - C_e)}{C_o} \times 100\% \tag{4}$$

where C_o and C_e are the initial and equilibrium concentration of metal ions (mg·L^{-1}), V (mL) is the volume of the system, and m (g) is the mass of CTS-*g*-B15C5 film.

The general expression for the distribution ratio k can be followed by Eq. (5) [33]:

$$k = \frac{(C_o - C_e)V}{C_o \times m} \quad (5)$$

where m is the mass of film (g), and V is the volume of solution containing metal ions (mL).

In order to investigate the adsorption selectivity, a selectivity coefficient ($K_{A/B}$) of two metal ions is defined by Eq. (6) [34]:

$$K_{A/B} = \frac{k_A}{k_B} \quad (6)$$

where k_A and k_B are the distribution ratio of the two metal ions.

3. Results and discussion

3.1. Characterization of CTS-g-B15C5

^{13}C NMR was used to characterize the chemical structure of CTS-*g*-B15C5. The solid-state ^{13}C NMR spectrum of CTS-*g*-B15C5 is shown in Fig. 1, and it was compared with solid-state ^{13}C NMR spectrum of CTS and ^{13}C NMR spectrum of CTS of FB15C5 (in CD_3Cl). In the spectrum of CTS (line 2 in Fig. 1), there were five main peaks at chemical shifts of 58.1, 61.0, 75.8, 83.1, and 105.3 ppm, which were ascribed to the six carbons in CTS bone, respectively. In the spectrum of FB15C5 (line 3 in Fig. 1), the peaks at chemical shifts of 110.8, 112.9, 126.8, 130.3, 149.5, and 154.5 ppm were belonging to the vibration of carbons on benzene ring, and the peaks at chemical shifts from 68.6 to 71.5 ppm and around 77.0 ppm were attribute to the carbons on crown ether ring. The characteristic peak of formyl group presented at 190.8 ppm. In the spectrum of CTS-*g*-B15C5 (line 1 in Fig. 1), the chemical shifts of the wide peak from 57.0 to 83.7 ppm were due to the abundant carbon on the backbone of CTS, and the peak at 70.9 ppm was ascribed to the carbons on crown ether ring. The chemical shifts from 104.8 to 152.1 ppm were ascribed to the six carbon of the benzene ring. The characteristic peak of C=N was presented at 166.3 ppm. The results obtained from ^{13}C NMR confirmed that a Schiff base type of CTS-*g*-B15C5 polymer was obtained.

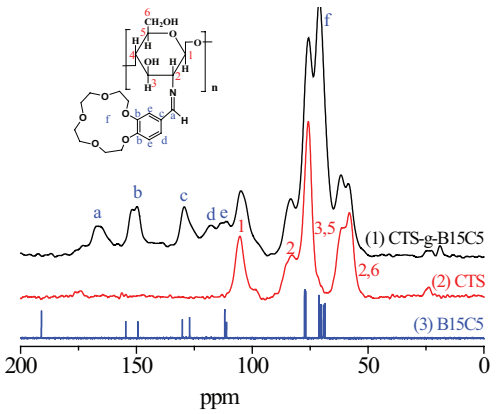

Fig. 1. ^{13}C NMR of CTS-*g*-B15C5 (solid state), CTS (solid state), and FB15C5 (in CD_3Cl).

3.2. Optimizing the experimental parameters for preparing CTS-g-B15C5

3.2.1. Model fitting

To study the interactive effects of different experimental parameters, the values of different reaction factors, the response values, and the experimental results are shown in Tables 1 and 2. The final quadratic equation that could indicate the relation between reaction factors and I_A according to the experiments obtained by Design Expert 8.0 was given in Eq. (7):

$$\begin{aligned} R = {} & 4.72 + 0.066 \times A - 0.10 \times B - 0.12 \times C - 0.10 \times D \\ & + 0.11 \times A \times B - 0.13 \times A \times C + 0.22 \times A \times D \\ & - 0.16 \times B \times C - 0.065 \times B \times D + 0.019 \times C \times D \\ & - 0.21 \times A^2 - 0.18 \times B^2 + 0.071 \times C^2 - 0.086 \times D^2 \end{aligned} \quad (7)$$

where R is the respond value (I_A). The impact factors A, B, C, and D refer to crown ether amount, ethanol amount, acetic acid concentration, and reaction time, respectively.

3.2.2. Analysis of variance

The results of the ANOVA for this response surface quadratic equation are shown in Table 3. It can be seen from Table 3 that the F value 3.66 is larger than the theoretical F value (2.48), which means that the model is significant. The low p value (<0.05) implies that the model terms are significant. The "lack of fit p-value" of 0.5841 (>0.05) indicates that the lack of fit is not significant and the model fits well. The R-squared (R^2 = 0.8220) reveals the goodness of the fit. Additionally, a relatively lower value of the coefficient of variances (C.V. [30] = 4.92%) reflects better accuracy and reliability of the experiments. "Adeq Precision" measures the ratio of signal to noise. Herein, the ratio of 7.472 indicates an adequate signal. Therefore, the present model can be used to navigate the design space.

Besides, ANOVA table can also be used to analyze the significant impact of various factors on the response value. The order of significant impact of single factor can compare by the size of F value: acetic acid concentration (C) > reaction time (D) > ethanol amount (B) > crown ether amount (A). Similarly, it can also found that the order of two factors interaction which influences on I_A was $AD > BC > AC > AB$.

3.2.3. Model adequacy testing

Fig. 2 shows the residual and the influence plots for the experiments. It can be found from Fig. 2(a) that the data tend to be close to a straight line and are consistent with the theoretical distribution. It indicates that the model obtained and the results of the ANOVA are reasonable and adequate. It also can be seen from Fig. 2(b) that the actual values are in good agreement with the predicted values.

Table 3
The ANOVA analysis of the model

Source	Sum of squares	Degrees of freedom	Mean square	*F* value	Probability level	
Model	1.45	14	0.1	3.66	0.0104	Significant
A	0.053	1	0.053	1.87	0.0193	
B	0.12	1	0.12	4.39	0.0547	
C	0.16	1	0.16	5.81	0.0303	
D	0.12	1	0.12	4.4	0.0547	
AB	0.046	1	0.046	1.62	0.0224	
AC	0.07	1	0.07	2.46	0.0139	
AD	0.2	1	0.2	7.11	0.0184	
BC	0.1	1	0.1	3.65	0.0767	
BD	0.017	1	0.017	0.6	0.0452	
CD	1.41×10^{-3}	1	1.41×10^{-3}	0.05	0.0826	
A^2	0.28	1	0.28	9.73	0.0075	
B^2	0.21	1	0.21	7.56	0.0157	
C^2	0.033	1	0.033	1.16	0.0299	
D^2	0.048	1	0.048	1.7	0.0213	
Residual	0.4	14	0.028			
Lack of fit	0.29	10	0.029	1.07	0.5841	Not significant
Pure error	0.11	4	0.027			
Core total	1.85	28				
C.V.% = 4.92		Adequate precision = 7.472		R^2 = 0.8220		

3.2.4. Significance analysis of influence factors

Taking two factors into account and keeping the other factors unchanged, a response surface about I_A vs. the factors can be obtained as shown in Fig. 3. It is observed from Fig. 3(a) that I_A increases with increasing the amount of crown ether and ethanol. Obviously, the contour plot of ethanol amount is much steeper than that of crown ether amount. It indicated that the influence of ethanol amount on I_A is greater than that of crown ether amount, which is in perfect accordance with the ANOVA.

Moreover, the effect of concentration of acetic acid and reaction time on I_A is presented in Fig. 3(b). The interactive effect of reaction time and acetic acid concentration is also highly significant. The influence of acetic acid concentration is greater than that of reaction time. Equally, the effect of reaction time and ethanol amount on I_A and their mutual interaction are illustrated in Fig. 3(c). As shown, the longer the reaction time, the higher I_A value. Obviously, the reaction time is a key factor for the reaction. Fig. 3(c) also shows that the influence of reaction time is greater than that of ethanol amount. The results from response surface analysis are consistent with the observations in section 3.2.2.

3.2.5. Optimization and validation

The maximum predicted value of I_A obtained by the BBD was 4.97 mmol·g^{-1} under the optimal conditions of 0.5 g CTS, 1.38 g crown ether, 33 mL ethanol as cosolvent, 8 wt% acetic acid as solvent, and reaction time 23 h. Three repeated validation experiments were implemented at the selected optimal levels of the operational parameters, and the average values of I_A were 4.93 mmol·g^{-1}, which is in good agreement with the predicted value. The results revealed that the BBD was a reliable and valuable method to optimize the amount of immobilized crown ether.

3.3. Adsorption properties

3.3.1. The adsorption property of FB15C5

As shown in Table 4, the adsorption rates of Pd^{2+} and Ag^{+} obtained by FB15C5 were 15.6% and 14.5%, respectively, and the order of adsorption ability for metal ions was $Pd^{2+} > Ag^{+} > Pb^{2+} > Cu^{2+} > Ni^{2+} > Cr^{3+}$. It is an interesting phenomenon that the adsorption capability of FB15C5 was relative to the metal ions radius (Table 5), which suggested that crown ethers could selectively adsorb metal ions. It is related to the cavity size and charge effect of crown ether cycle on FB15C5. On one hand, the center of crown ether (B15C5) bears a negative charge. Therefore, a host–guest complex would be formed by electrostatic interaction between crown ether and cation (metal ion). On the other hand, when the interior cavity ("hole") size of crown ether molecule is near to that of a given cation, the binding between crown ether and the cation is proper. This is the so-called "hole size relationship". For instance, the cavity radius of B15C5 is approximately 0.8–1.1 Å [35]. As shown in Table 6, the ionic radii of Ag^{+} and Pd^{2+} are 1.21 and 0.85 Å, which are close to that of B15C5. Consequently, FB15C5 was apt to adsorb Ag^{+} and Pd^{2+}.

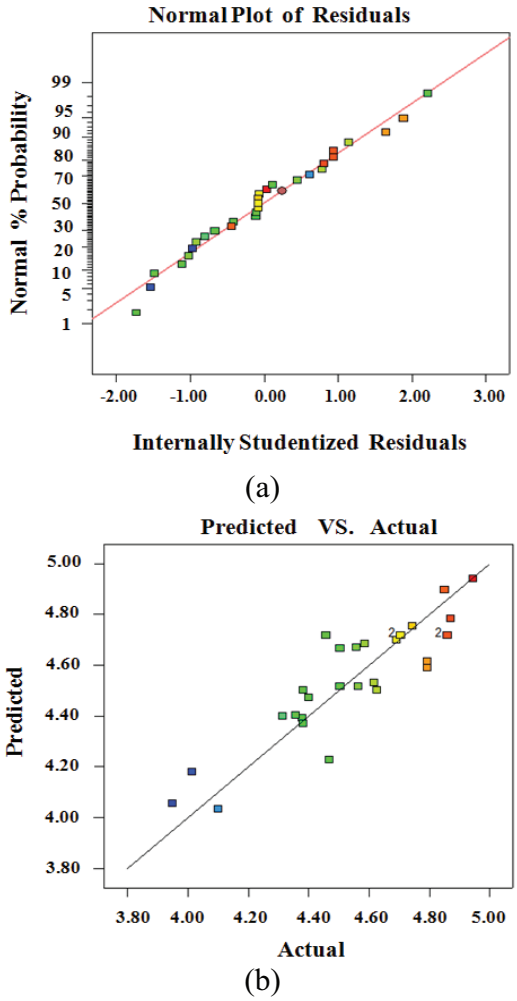

Fig. 2. Normal probability graph of internal residuals (a) and predicted vs. actual plot (b).

3.3.2. The adsorption property of CTS and CTS-g-B15C5

It is well known that CTS can form complexes with various metal ions. The amino groups on the chain are involved in specific interactions with metals [37]. As shown in Table 4, CTS exhibited good adsorption for many metal ions, especially for Cu^{2+}. The affinity of CTS for cations may be explained by "Pendant Model" proposed by Ogawa and Oka [38]. However, it is obvious in Table 4 that the adsorption capability for Ni^{2+}, Cu^{2+}, and Cr^{3+} sharply decreased while that for Ag^{+} and Pd^{2+} steadily increased after the crown ether being graft onto CTS. The decrease of adsorption capability for Ni^{2+}, Cu^{2+}, and Cr^{3+} may be due to inactivation of $-NH_2$ groups, while the increase of adsorption capability for Ag^{+} and Pd^{2+} may be ascribed to the highly selective complexation of B15C5 on CTS with metal ions. As shown in Table 4, the adsorption capability of CTS-*g*-B15C5 is much higher than that of FB15C5. Especially, the adsorption rates of CTS-*g*-B15C5 was 94.3% for Pd^{2+} and 96.9% for Ag^{+} as a result of a synergistic effect between CTS main chain and B15C5 during the solid–liquid extraction. The results obtained were in good agreement with those reported by Gokel et al. [39].

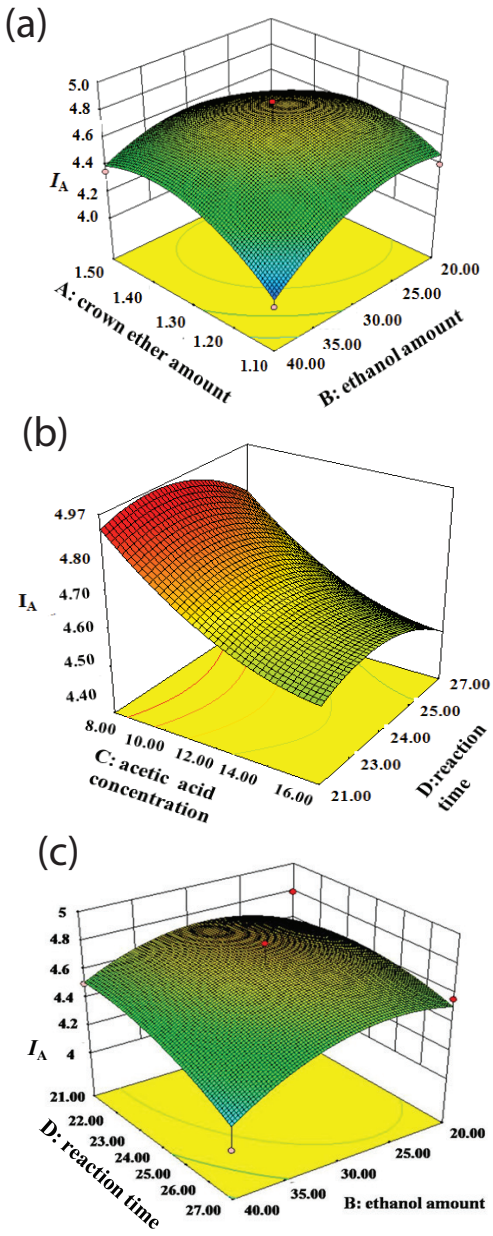

Fig. 3. Three-dimensional (3D) response surface for immobilized amount of crown ether: (a) the interaction of crown ether amount and ethanol amount; (b) the interaction of acetic acid concentration and reaction time; and (c) the interaction of ethanol amount and reaction time.

Table 4
The adsorption rate of FB15C5, CTS, and CTS-*g*-B15C5[a]

Adsorbent	Adsorption rate (%)					
	Pb^{2+}	Ag^{+}	Pd^{2+}	$^{Ni}2+$	Cu^{2+}	Cr^{3+}
FB15C5	12.6	14.5	15.6	1.7	2.3	1.8
CTS	67.3	90.9	59.7	47.1	96.3	60.6
CTS-B15C5	72.4	96.9	94.3	17.8	24.6	11.2

[a]pH value was 4.0 [32] and the adsorption time was 12 h.

In sum, both CTS and CTS-*g*-B15C5 present the different selectivity to different heavy metal ions. The further explanations about the adsorption selectivity of CTS and CTS-*g*-B15C5 would be illustrated in the following section.

3.3.3. The adsorption selectivity of CTS and CTS-g-B15C5

The selectivity coefficient of two ions is the most useful parameter during the practical applications of adsorption materials. The selectivity coefficients of CTS and CTS-*g*-B15C5 for metal ions are listed in Table 6.

As mentioned in section 3.3.2, CTS is an excellent natural adsorbent for metal ions due to the presence of $-NH_2$ and –OH groups. However, CTS shows poor adsorption selectivity. For instance, as shown in Table 6, the selectivity coefficients for CTS are $K_{Ag^+/Ni^{2+}}$ = 2.06, $K_{Ag^+/Cr^{3+}}$ = 1.60, and $K_{Pd^{2+}/Cr^{3+}}$ = 0.99. On contrary, the selectivity coefficients of metal ions for CTS-*g*-B15C5 are much higher than those for CTS. For example, the coefficients of selectivity of metal ions for CTS-*g*-B15C5 are $K_{Ag^+/Ni^{2+}}$ = 5.40, $K_{Ag^+/Cr^{3+}}$ = 8.59, and $K_{Pd^{2+}/Cr^{3+}}$ = 8.44, respectively. The reason is that crown ether exhibits selective adsorption for particular ions with proper radius and charge so as to form a complex. As shown in Fig. 4, it could be seen from the structure model of Ag^+–(CTS-*g*-B15C5) complex that the crown ether segment on CTS-*g*-B15C5 coordinated with Ag^+ by one-to-one [40]. It is possible that Ag^+ not only sit on top of the B15C5 plane slightly, but also coordinated with five oxygen atoms of crown ether cycle and one oxygen atom nearby of CTS main chain, thus to form a pseudo-octahedral structure. Such a complex is known to be relatively more stable than the complex formed through the coordination with only B15C5.

Table 5
The radius of different metal ions [36]

Metal ion	Radius (Å)
Pb^{2+}	1.27
Ag^+	1.21
Pd^{2+}	0.85
Ni^{2+}	0.73
Cu^{2+}	0.72
Cr^{3+}	0.62

Table 6
The selectivity coefficient of CTS and CTS-*g*-B15C5

Adsorbent	CTS	CTS-*g*-B15C5
$K_{Ag^+/Ni^{2+}}$	2.06	5.40
$K_{Ag^+/Cr^{3+}}$	1.60	8.59
$K_{Pd^{2+}/Ni^{2+}}$	1.27	5.31
$K_{Pd^{2+}/Cr^{3+}}$	0.99	8.44
$K_{Pb^{2+}/Ni^{2+}}$	1.64	4.07
$K_{Pb^{2+}/Cr^{3+}}$	1.28	6.47

3.3.4. Kinetics and isotherm adsorption studies

The effect of time on the adsorption rate of Ag^+ and Pd^{2+} ions on CTS-*g*-B15C5 film is shown in Fig. 5. It can be seen that the adsorption capacity increased dramatically at the first 2 h, then reached a plateau after the adsorption time of 4 h. The equilibrium adsorption rate was up to 96.9% and 94.3% for Ag^+ and Pd^{2+}, respectively. The pseudo-first-order adsorption kinetic model (Eq. (8)) was used to characterize the adsorption process as shown in Fig. 5.

$$\ln(q_e - q_t) = \ln q_e - kt \tag{8}$$

where q_t and q_e are the adsorption rate of the CTS-*g*-B15C5 film at adsorption time t and equilibrium, respectively. k is the rate constant of the pseudo-first-order adsorption kinetic model.

According to Eq. (6), the calculated rate constant k was 1.83 and 0.92 h^{-1}, and the calculated adsorption rate of the CTS-*g*-B15C5 film at adsorption equilibrium was 96.5% and 94.9%, which are in agreement with the actual value of adsorption rate as shown in Fig. 5.

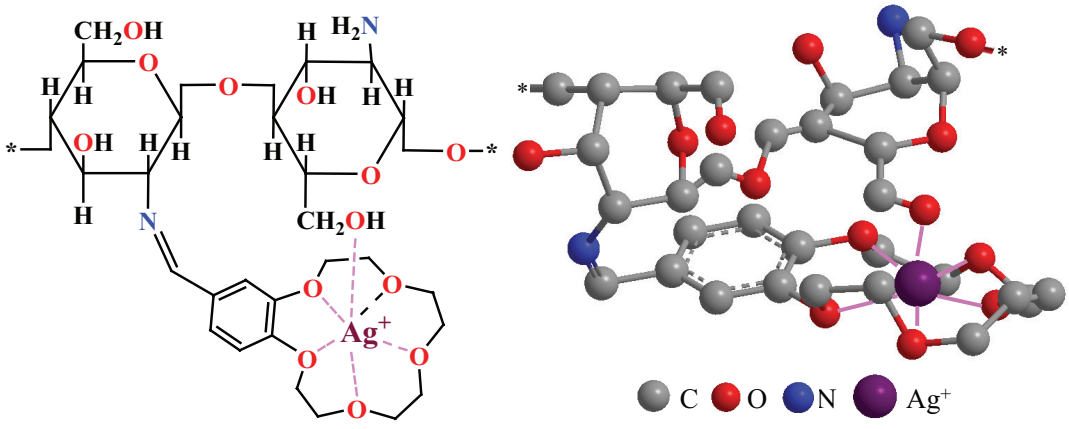

Fig. 4. Structure models of Ag^+-CTS-*g*-B15C5 complex.

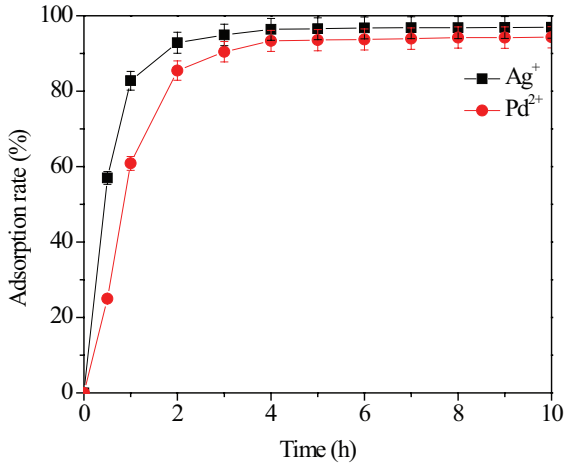

Fig. 5. Adsorption kinetics of Ag^+ and Pd^{2+} ions on CTS-*g*-B15C5 film.

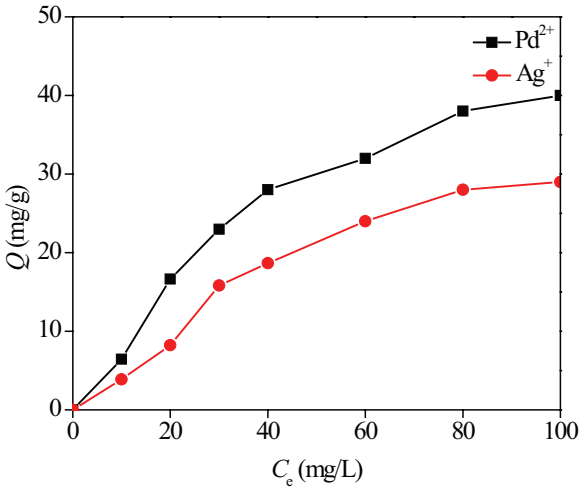

Fig. 6. Adsorption isotherms of Ag^+ and Pd^{2+} ions on CTS-*g*-B15C5 film.

The adsorption isotherms of Ag^+ and Pd^{2+} ions on CTS-*g*-B15C5 film are shown in Fig. 6. The isotherm data of the both ions can be fitted well by the Langmuir model (Eq. (9)). The regression coefficients (R^2) were 0.988 and 0.979 for Ag^+ and Pd^{2+} ions, respectively. These results indicated a monolayer adsorption process.

$$Q_e = Q_m \frac{bC_e}{1+bC_e} \tag{9}$$

where Q_e (mg·g^{-1}) is the adsorption amount at equilibrium, Q_m (mg·g^{-1}) is the adsorption theoretical monolayer adsorption capacity of the adsorbent, C_e (mg·L^{-1}) is the equilibrium ions concentration in solution, b is the Langmuir constant and related to the free energy of adsorption.

3.3.5. The reusability of CTS-g-B15C5

Thiourea was used to regenerate the used CTS-*g*-B15C5 film. The used CTS-*g*-B15C5 film was washed with excess thiourea solution (0.01 mol·L^{-1}) and water until no metal ions were detected in the washed water. The regenerated film was reused in the next adsorption experiment with the same condition as before to examine the reusability of CTS-*g*-B15C5 film. Fig. 7 shows the adsorption capacity of the used CTS-*g*-B15C5 film for Ag^+ and Pd^{2+}. It was seen that the film showed good adsorption performance after regeneration. The adsorption rates for Ag^+ and Pd^{2+} were more than 90% after being regenerated for five times, which suggests a good stability of the CTS-*g*-B15C5 film.

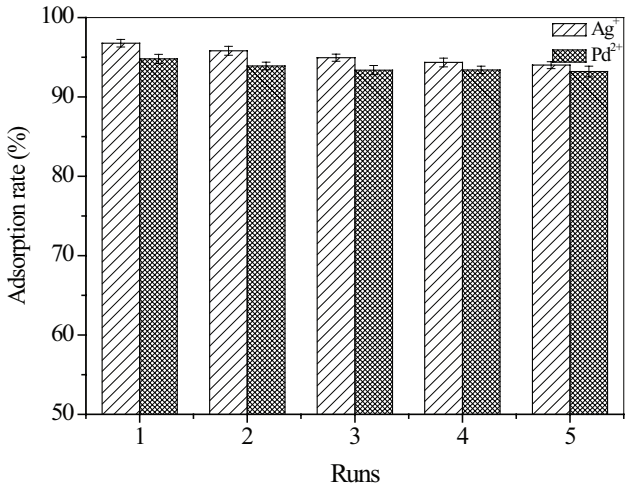

Fig. 7. Adsorption rate of the regenerated CTS-*g*-B15C5 film for Ag^+ and Pd^{2+}.

4. Conclusions

CTS-*g*-B15C5 film for metal ion separation was prepared. The grafting reaction parameters were optimized by BBD, and the predicted immobilized amount of crown ether was 4.97 mmol·g^{-1}, which was in agreement with the actual value (4.93 mmol·g^{-1}). CTS-*g*-B15C5 exhibited higher adsorption ability for Pd^{2+} and Ag^+ owning to the synergistic effect of the crown ether group and CTS. The adsorption rates obtained by CTS-*g*-B15C5 film were 96.9% for Ag^+ and 94.3% for Pd^{2+}, and the selectivity coefficients of CTS-*g*-B15C5 for metal ions were $K_{Ag^+/Ni^{2+}} = 5.40$, $K_{Ag^+/Cr^{3+}} = 8.59$, and $K_{Pd^{2+}/Cr^{3+}} = 8.44$, respectively. Furthermore, the adsorption rates for Ag^+ and Pd^{2+} were more than 90% after being regenerated for five times. The results indicated that CTS-*g*-B15C5 film could be used for separation of precious metals Ag^+ and Pd^{2+}.

Acknowledgments

The authors gratefully acknowledge the financial support by the National Natural Science Foundation of China (Grant No. 51303130, 21376176, and 21174104), China Scholarship Council and the Program for Changjiang Scholars and Innovative Research Team in University (PCSIRT) of Ministry of Education of China (Grant No. IRT13084), and the Science and Technology Plans of Tianjin (No. 16PTSYJC00100).

References

[1] W. Sliwa, T. Girek, Metallocyclodextrins and related species, Heterocycles, 60 (2003) 2147–2183.

[2] K.K. Bhatluri, M.S. Manna, P. Saha, A.K. Ghoshal, Supported liquid membrane-based simultaneous separation of cadmium and lead from wastewater, J. Membr. Sci., 459 (2014) 256–263.

[3] K. Lisha, S.M. Maliyekkal, T. Pradeep, Manganese dioxide nanowhiskers: a potential adsorbent for the removal of Hg(II) from water, Chem. Eng. J., 160 (2010) 432–439.

[4] S. Khaoya, U. Pancharoen, Removal of lead (II) from battery industry wastewater by HFSLM, Int. J. Chem. Eng. Appl., 3 (2012) 98–103.

[5] H.A. Aziz, M.N. Adlan, K.S. Ariffin, Heavy metals (Cd, Pb, Zn, Ni, Cu and Cr(III)) removal from water in Malaysia: post treatment by high quality limestone, Bioresour. Technol., 99 (2008) 1578–1583.

[6] S.I. Park, I.S. Kwak, S.W. Won, Y.-S. Yun, Glutaraldehyde-crosslinked chitosan beads for sorptive separation of Au(III) and Pd(II): opening a way to design reduction-coupled selectivity-tunable sorbents for separation of precious metals, J. Hazard. Mater., 248 (2013) 211–218.

[7] M.J.K. Ahmed, M. Ahmaruzzaman, A review on potential usage of industrial waste materials for binding heavy metal ions from aqueous solutions, J. Water Process Eng., 10 (2016) 39–47.

[8] M. Naushad, A. Mittal, M. Rathore, V. Gupta, Ion-exchange kinetic studies for Cd(II), Co(II), Cu(II), and Pb(II) metal ions over a composite cation exchanger, Desal. Wat. Treat., 54 (2015) 2883–2890.

[9] V.K. Thakur, S.I. Voicu, Recent advances in cellulose and chitosan based membranes for water purification: a concise review, Carbohydr. Polym., 146 (2016) 148–165.

[10] M. Al-Shannag, Z. Al-Qodah, K. Bani-Melhem, M.R. Qtaishat, M. Alkasrawi, Heavy metal ions removal from metal plating wastewater using electrocoagulation: kinetic study and process performance, Chem. Eng. J., 260 (2015) 749–756.

[11] M.I. Inyang, B. Gao, Y. Yao, Y. Xue, A. Zimmerman, A. Mosa, P. Pullammanappallil, Y.S. Ok, X. Cao, A review of biochar as a low-cost adsorbent for aqueous heavy metal removal, Crit. Rev. Environ. Sci. Technol., 46 (2016) 406–433.

[12] S.E. Bailey, T.J. Olin, R.M. Bricka, D.D. Adrian, A review of potentially low-cost sorbents for heavy metals, Water Res., 33 (1999) 2469–2479.

[13] C.D. Tran, S. Duri, A. Delneri, M. Franko, Chitosan-cellulose composite materials: preparation, characterization and application for removal of microcystin, J. Hazard. Mater., 252 (2013) 355–366.

[14] W.W. Ngah, C. Endud, R. Mayanar, Removal of copper(II) ions from aqueous solution onto chitosan and cross-linked chitosan beads, React. Funct. Polym., 50 (2002) 181–190.

[15] M. Suguna, N. Siva Kumar, A. Subba Reddy, V. Boddu, A. Krishnaiah, Biosorption of lead(II) from aqueous solution on glutaraldehyde cross-linked chitosan beads, Can. J. Chem. Eng., 89 (2011) 833–843.

[16] M. Sadeghi-Kiakhani, M. Arami, K. Gharanjig, Preparation of chitosan-ethyl acrylate as a biopolymer adsorbent for basic dyes removal from colored solutions, J. Environ. Chem. Eng., 1 (2013) 406–415.

[17] A.A. Tayel, M.M. Gharieb, H.R. Zaki, N.M. Elguindy, Bio-clarification of water from heavy metals and microbial effluence using fungal chitosan, Int. J. Biol. Macromol., 83 (2016) 277–281.

[18] N. Alves, J. Mano, Chitosan derivatives obtained by chemical modifications for biomedical and environmental applications, Int. J. Biol. Macromol., 43 (2008) 401–414.

[19] R.S. Vieira, M.M. Beppu, Interaction of natural and crosslinked chitosan membranes with Hg(II) ions, Colloids Surf., A, 279 (2006) 196–207.

[20] S. Lu, H. Li, F. Zhang, N. Du, W. Hou, Sorption of Pb(II) on carboxymethyl chitosan-conjugated magnetite nanoparticles: application of sorbent dosage-dependent isotherms, Colloid Polym. Sci., 294 (2016) 1369–1379.

[21] L. Zhang, L. Zhong, S. Yang, D. Liu, Y. Wang, S. Wang, X. Han, X. Zhang, Adsorption of Ni(II) ion on Ni(II) ion-imprinted magnetic chitosan/poly(vinyl alcohol) composite, Colloid Polym. Sci., 293 (2015) 2497–2506.

[22] R.K. Katarina, T. Takayanagi, M. Oshima, S. Motomizu, Synthesis of a chitosan-based chelating resin and its application to the selective concentration and ultratrace determination of silver in environmental water samples, Anal. Chim. Acta, 558 (2006) 246–253.

[23] Z. Liu, H. Wang, C. Liu, Y. Jiang, G. Yu, X. Mu, X. Wang, Magnetic cellulose–chitosan hydrogels prepared from ionic liquids as reusable adsorbent for removal of heavy metal ions, Chem. Commun., 48 (2012) 7350–7352.

[24] N.G. Kandile, A.S. Nasr, Environment friendly modified chitosan hydrogels as a matrix for adsorption of metal ions, synthesis and characterization, Carbohydr. Polym., 78 (2009) 753–759.

[25] S. Ding, X. Zhang, X. Feng, Y. Wang, S. Ma, Q. Peng, W. Zhang, Synthesis of *N,N′*-diallyl dibenzo 18-crown-6 crown ether crosslinked chitosan and their adsorption properties for metal ions, React. Funct. Polym., 66 (2006) 357–363.

[26] R.A. Samant, V.S. Ijeri, A.K. Srivastava, Complexation of macrocyclic compounds with metal ions: 2. Mg(II), Ca(II), Sr(II), Ba(II), Cu(II), and Ag(I) in 20 mass propylene carbonate ethylene carbonate, J. Chem. Eng. Data, 48 (2003) 203–207.

[27] T. Zhang, F. Yan, J. Li, B. He, W. Leng, D. Guo, Z. Cui, Preparation and characterization of chitosan graft 4′-formoxylbenzo-15-crown-5-ether for lithium isotopes separation, Chin. J. Colloid Polym., 33 (2015) 3–6.

[28] M. Lavertu, Z. Xia, A. Serreqi, M. Berrada, A. Rodrigues, D. Wang, M. Buschmann, A. Gupta, A validated ^{1}H NMR method for the determination of the degree of deacetylation of chitosan, J. Pharm. Biomed. Anal., 32 (2003) 1149–1158.

[29] R. Ungaro, B. El Haj, J. Smid, Substituent effects on the stability of cation complexes of 4′-substituted monobenzo crown ethers, J. Am. Chem. Soc., 98 (1976) 5198–5202.

[30] S. Zhu, Y. Li, C.-y. Ma, Z.-x. Lou, S.-w. Chen, J. Dai, H.-x. Wang, Optimization of lipase-catalyzed synthesis of acetylated EGCG by response surface methodology, J. Mol. Catal. B: Enzym., 97 (2013) 87–94.

[31] P. Sharma, L. Singh, N. Dilbaghi, Optimization of process variables for decolorization of Disperse Yellow 211 by *Bacillus subtilis* using Box–Behnken design, J. Hazard. Mater., 164 (2009) 1024–1029.

[32] M.L. Cervera, M.C. Arnal, M. de la Guardia, Removal of heavy metals by using adsorption on alumina or chitosan, Anal. Bioanal. Chem., 375 (2003) 820–825.

[33] X. Yuan, J. Liu, G. Zeng, J. Shi, J. Tong, G. Huang, Optimization of conversion of waste rapeseed oil with high FFA to biodiesel using response surface methodology, Renew. Energy, 33 (2008) 1678–1684.

[34] X. Wang, L. Zhang, C. Ma, R. Song, H. Hou, D. Li, Enrichment and separation of silver from waste solutions by metal ion imprinted membrane, Hydrometallurgy, 100 (2009) 82–86.

[35] H.K. Frensdorff, Stability constants of cyclic polyether complexes with univalent cations, J. Am. Chem. Soc., 93 (1971) 600–606.

[36] T.M. Mututuvari, C.D. Tran, Synergistic adsorption of heavy metal ions and organic pollutants by supramolecular polysaccharide composite materials from cellulose, chitosan and crown ether, J. Hazard. Mater., 264 (2014) 449–459.

[37] M. Rinaudo, Chitin and chitosan: properties and applications, Prog. Polym. Sci., 31 (2006) 603–632.

[38] K. Ogawa, K. Oka, T. Yui, X-ray study of chitosan-transition metal complexes, Chem. Mater., 5 (1993) 726–728.

[39] G.W. Gokel, W.M. Leevy, M.E. Weber, Crown ethers: sensors for ions and molecular scaffolds for materials and biological models, Chem. Rev., 104 (2004) 2723–2750.

[40] M.A. Siegler, J.H. Prewitt, S.P. Kelley, S. Parkin, J.P. Selegue, C.P. Brock, More examples of the 15-crown-5···H_2O—M—OH_2···15-crown-5 motif, M = Al^{3+}, Cr^{3+} and Pd^{2+}, Acta Crystallogr., Sect. B, 66 (2010) 213–221.